Applied Catalysis B: Environmental 91 (2009) 144–151

Contents lists available at ScienceDirect

Applied Catalysis B: Environmental

journal homepage: www.elsevier.com/locate/apcatb

NH_3 formation and utilization in regeneration of $Pt/Ba/Al_2O_3$ NO_x storage-reduction catalyst with H_2

William P. Partridge *, Jae-Soon Choi

Fuels, Engines, and Emissions Research Center, Oak Ridge National Laboratory, 2360 Cherahala Blvd., Knoxville, TN 37932, USA

ARTICLE INFO

Article history:
Received 3 February 2009
Received in revised form 8 May 2009
Accepted 12 May 2009
Available online 20 May 2009

Keywords:
LNT
Regeneration
NH_3
Intra-catalyst measurements
SpaciMS

ABSTRACT

The nature of H_2 regeneration of a model $Pt/Ba/Al_2O_3$ LNT catalyst was investigated with specific focus on intra-catalyst formation and utilization of NH_3 and its role in catalyst regeneration. In situ measurements of the transient intra-catalyst species (H_2, NH_3, N_2, NO_x) distributions at different temperatures were used to detail the reaction evolution along the catalyst axis. Comparison of the species transients identifies unique individual natures for the reductant (H_2), inert product (N_2) and intermediate-reductant product (NH_3) which readily explain the conventional effluent species sequence as an integral effect. The data demonstrate that NH_3 is created on similar timescales as the N_2 product inside the catalyst, but consumed as aggressively as H_2 reductant along the catalyst. This spatiotemporal NH_3 behavior experimentally confirms that Intermediate-NH_3 regeneration pathway is active. Analysis at 200 and 325 °C indicates equivalent local NO_x storage, H_2 consumption and regeneration effectiveness, but differing NH_3/N_2 ratio, suggesting a temperature-dependence of partitioning between Direct-H_2 and Intermediate-NH_3 regeneration pathways. Further experimental and numerical work is needed to more clearly understand the partitioning between the possible regeneration pathways. Nevertheless, the experimental data show that intermediate NH_3 plays a significant role in LNT catalyst regeneration.

1. Introduction

Lean NO_x trap (LNT) or NO_x storage-reduction (NSR) catalysts provide an aftertreatment methodology for reducing NO_x emissions from lean burn diesel or gasoline engines [1]. The LNT catalyst formulations typically contain storage components such as Ba or K and precious metals such as Pt dispersed on alumina support of high-surface area; but can also contain other components including Ce for oxygen storage capacity (OSC) or as a support. LNT catalysts function by storing NO_x (e.g., as barium nitrate) during normal lean combustion operation, and periodically regenerating the catalyst to convert the stored NO_x to N_2 and refresh the storage capacity of the catalyst. Regeneration is effected by changing the engine operation to create net reducing conditions in the exhaust, and supply the LNT catalyst with a broad reductant pool including H_2, CO and various hydrocarbons. Effective regeneration strategies strive to achieve high N_2 selectivity while minimizing other nitrogen-containing emissions such as NH_3 and N_2O.

Ammonia reactions and slip from NSR catalyst during regeneration have been observed and studied [2–13]. Ammonia can be toxic, cause lung irritation, and potentially more acute health consequences [14]. Mobile sources, primarily gasoline vehicles with three-way catalysts, are the most significant sources of NH_3 in urban air [15]. In ambient air, NH_3 forms secondary aerosols of ammonium sulfate and ammonium nitrate by gas-to-particle conversion mechanisms involving oxides of nitrogen and sulfur [16]. These aerosols are an important contributor to urban fine particulate ($PM_{2.5}$) pollution [16]. The need to avoid NH_3 slip from NSR catalysts has driven studies to better understand the NH_3 formation and utilization mechanisms in NSR catalysis. Typically, catalyst effluent NH_3 slip is observed at the end of regeneration after nitrogen selectivity ($2[N_2]/\{[NO_x] + 2[N_2] + 2[N_2O] + [NH_3]\}$) begins to decrease. Based on this effluent emissions sequence and the catalyst-emissions nature at varying NO_x loadings, temperatures and H_2 concentrations, Nova et al. [4,7] suggested a reaction scheme where regeneration of nitrates adjacent to Pt (i.e., "fast NO_x storage sites") occurs first with high N_2 selectivity, while nitrates less proximal to Pt (i.e., "slow NO_x storage sites") are regenerated later with higher NH_3 selectivity. Pihl et al. [6] studied LNT product selectivity, and found NH_3 formation favored at high reductant-to-NO_x ratios and lower temperatures. Noting that NH_3 is known as an effective reductant for both NO and NO_2, this group noted that NH_3 formed in one portion of the catalyst could be consumed in another portion of the NSR catalyst via regeneration reactions or reduction

* Corresponding author. Tel.: +1 865 946 1234; fax: +1 865 946 1354.
E-mail address: partridgewp@ornl.gov (W.P. Partridge).

0926-3373/$ – see front matter © 2009 Elsevier B.V. All rights reserved.
doi:10.1016/j.apcatb.2009.05.017

of stored oxygen; the possibility of oxidation of NH_3, breaking through the regeneration front, to N_2O was also included. In the resulting conceptual model, NH_3 is formed at the reductant front at low temperatures and by "slow" nitrate sites behind the reductant front; Pihl et al. specifically emphasized the importance of slow sites which is consistent with the work of Nova et al. Ribeiro and co-workers [8,9] made a major step in suggesting that NSR catalyst regeneration with H_2 can actually occur through intermediate NH_3 formation. This group concluded that LNT regeneration is controlled by reductant supply and is not mass transfer or kinetically limited, and downplayed the significance of LNT regeneration via NH_3 formed at "slow sites." In both the works of Pihl et al. [6] and Ribeiro et al. [9], the integral nature of the NSR catalyst is emphasized in their figures and conceptual models. Nova et al. [11] have shown that NH_3 can directly regenerate stored NO_x via Pt-catalyzed reaction not involving gaseous NO, and suggest a two-step regeneration pathway involving fast formation of NH_3 from reaction of H_2 with stored NO_x, and subsequent slower reaction of this NH_3 and stored NO_x with high N_2 selectivity. In subsequent work, Lietti et al. [12] propose that N_2 is formed exclusively via this "in-series two-step" pathway. The works cited above convey a complex network of NH_3 formation and utilization reactions in different zones along the catalyst channel. This complexity is exacerbated by the limitations of catalyst effluent measurements, which are unable to resolve variations along the catalyst channel. In fact, the concept of "slow sites" might be explained by integral effects and the limitations of effluent measurements. Transient intra-catalyst measurements of NH_3 and the species pool partitioning along the catalyst channel could provide critical insight into the various NH_3 roles in NSR regeneration outlined above.

Direct evidence of parallel Direct-H_2 and Intermediate-NH_3 regeneration pathways has been recently provided by Clayton et al. [13]. In this work, the intra-catalyst species pool evolution was reconstructed from effluent measurement of different length catalyst sections. The data is consistent with NH_3 being produced and consumed along the catalyst and thus functioning as an intermediate reductant. Further clarification of LNT NH_3 chemistry could be achieved by obtaining additional intra-catalyst data with greater spatiotemporal resolution under practically relevant conditions (fast cycling, range of temperatures, presence of H_2O and CO_2).

In recent work we made intra-catalyst measurements using spatially resolved capillary inlet mass spectrometry (SpaciMS) [17] to investigate the impact of sulfation on various LNT catalyst reactions including NSR and OSC [10], and used the resulting insights to explain the response of NH_3 slip to sulfation. With respect to the NSR function, sulfation had a plug-like front, and NSR was effectively inactive in the sulfated region. On the contrary, sulfation only degraded OSC in the sulfated region, and the sulfation front was more spatially distributed with respect to the OSC function. Based on this work, we extended the conceptual model of Pihl et al. [6] to explain increasing NH_3 slip with increasing LNT sulfation. In this model, an OSC-only zone exists, downstream of the NSR region, where NH_3 slipping through the NSR region is oxidized. As sulfation progresses, the NSR region is continually displaced further down the catalyst axis, correspondingly reducing the OSC-only zone, and thus the capacity to oxidize NH_3 created upstream. As a result of this shortening OSC-only zone, NH_3 slip increases with sulfation. This expanded conceptual model was based on transient intra-LNT measurements of NO_x and H_2 distributions, and NH_3 was not directly measured. This model suggests that NH_3 should continually decrease through the OSC-only zone. Direct intra-catalyst measurements of the transient NH_3 distribution are needed to investigate our sulfation model.

Ammonia can be used to convert NO_x in selective-catalytic-reduction (SCR) catalysts, and hybrid LNT–SCR systems based on discrete [18] and integrated [19] components have been proposed. In these hybrid systems, NH_3 generated in the LNT component is stored in the SCR component and used for additional NO_x reduction. In this mode it may be desirable to generate NH_3 in the LNT component to charge the SCR catalyst. This is a major step beyond simply avoiding NH_3 slip from LNT catalysts, and points to the need for a more detailed understanding of NH_3 generation and utilization in LNT catalysts in order to effectively design and operate hybrid LNT–SCR catalyst systems.

While SpaciMS has enabled many unique insights via intra-catalyst measurements [10,20–23], SpaciMS measurements of transient NH_3 distributions can be difficult. Specifically, NH_3 has interferences with abundant exhaust species including N_2, H_2O and NO_x. The polarity of NH_3 creates wall effects throughout the instrument which can temporally broaden NH_3 transient measurements; this is more dramatic but similar to the wall effects observed for other polar compounds like NO_2. Furthermore, there are chromatography effects unique to the direct capillary sampling methodology used with SpaciMS that must be considered in temporally aligning NH_3 transients with the other major species transients. Breen et al. [24] have addressed some of these issues and demonstrated fast transient measurements of NH_3. However, intra-catalyst NH_3 measurements have not been demonstrated, and additional measurement considerations may be required for SpaciMS measurements.

The focus of this paper is on understanding the intra-catalyst formation and utilization of NH_3, and specifically on its role in catalyst regeneration. We demonstrate SpaciMS measurements of transient NH_3 distributions within an operating LNT catalyst at different operation temperatures. In addition to transient NH_3 distributions, NO_x, N_2 and H_2 were also measured. The timescales of NH_3 generation and NO_x reduction reactions and the selectivity distributions were quantified. This work provides the foundation for assessing and improving the current understanding of lean NO_x trap catalysis. In particular, this work provides further insights on the existence and extent of intermediate NH_3 generation and utilization during LNT regeneration under realistic cycling conditions with high spatiotemporal resolution.

2. Experimental

The catalyst used in this work was a $Pt/Ba/Al_2O_3$ model LNT formulation washcoated on a honeycomb cordierite monolith (46.5 cells per cm^2) and provided by EmeraChem. The Pt and BaO loadings were 6.2 and 15 g L^{-1} estimated from the ICP-AES (Inductively Coupled Plasma-Atomic Emission Spectrometry) measurements. The washcoat was based on high-surface area Al_2O_3 (alumina surface area = ca. 160 m^2 g^{-1}). The percentage of Pt atoms exposed was estimated to be 15% based on the number of H atoms irreversibly adsorbed at room temperature, while the BET surface area of the catalyst (washcoat + cordierite) was determined to be 14 m^2 g^{-1} from Ar adsorption at 77 K. A core (2.1-cm diameter and 7.6-cm long) of the catalyst was evaluated in a bench-scale flow reactor. The reactor, which exposed the catalyst cores to synthetic exhaust under realistic cycling conditions, has been described previously [10,20,21,23]. The catalyst core was wrapped in Zetex insulating tape and mounted in a quartz reactor tube which was housed in an electric tube furnace. Mass flow controllers were used to meter bottled gasses (ultra high purity grade, Air Liquide), an evaporation system provided controlled H_2O concentration, and a four-way valve provided rapid (<0.2 s) switching for lean/rich/lean cycling. Short lean/rich cycling (60-s lean and 5-s rich) was used to study catalyst NH_3 chemistry under realistic conditions. Lean-phase composition included 300 ppm

NO and 10% O_2; rich-phase composition included 2% H_2; and 5% H_2O, 5% CO_2, 100 ppm Kr and Ar balance were common to both the lean and rich cycle phases. Catalyst evaluation was performed at three temperatures (200, 325 and 400 °C) based on the catalyst mid-channel temperature.

Catalyst temperature and effluent gas composition were determined via thermocouples and FTIR, respectively. Type-K thermocouples were used to measure the inlet (1-mm diameter) and outlet (0.5-mm diameter) at ca. 0.6 cm axially from the monolith faces, and catalyst mid-channel (0.5-mm diameter) temperatures. An FTIR gas analyzer (Midac M2000) measured NO, NO_2, N_2O, NH_3, CO, CO_2, and H_2O in the catalyst effluent.

Intra-catalyst gas phase speciation was performed by using SpaciMS developed in house [10,17,20–23]. The SpaciMS used in this study was based on a quadrupole mass filter (Pfeiffer, Prisma QMA200), with an oven-housed 12-port capillary inlet system. Deactivated capillary (50-μm ID, 220-μm OD, 3-m long; SGE International) was used for minimally invasive (sampling rate: ca. 10 μL min^{-1}) intra-catalyst SpaciMS sampling for the work reported here. For this work a single capillary was translated along a single catalyst channel to resolve the transient species distributions associated with lean/rich LNT cycling. Capillary translation with sub-millimeter resolution was achieved by using a stepper-motor-driven translation stage (Velmex, UniSlide) housed in a second oven. The capillary was housed in a heated hose between the multi-port-valve and translation oven. The SpaciMS capillary was inserted into the quartz tube housing the catalyst core on the centerline and from the gas-inlet end. The capillary was housed in a heated guide tube between the translation oven and up to within ca. 3 mm before the catalyst inlet face. The quadrupole, valve oven, heated hose and translation-stage oven were maintained at 80, 120, 120 and 60 °C, respectively. The intra-catalyst capillary and thermocouple were positioned in adjacent catalyst channels. In addition to catalyst inlet (0*L*, where *L* is the catalyst-core length) and outlet (1*L*) SpaciMS measurements, calibration measurements were made by positioning the capillary tip 2 mm before the catalyst inlet face (−2 mm). Intra-catalyst channel measurements were made at 11 locations; these were in 0.042*L* (*L*/24, 3.175 mm) increments from the inlet face up to 0.25*L* (19.05 mm from the inlet face), and in 0.125*L* (*L*/8, 9.525 mm) increments in the back 0.75*L* of the catalyst core. To accommodate signal-level disparities, separate scans were performed to measure the H_2 and N species. Measurements were made at m/z 2 (H_2), m/z 14 (N_2, NH_3, NO_x = NO + NO_2), m/z 15 (NH_3, NO_x), m/z 30 (NO_x) and m/z 84 (Kr). In addition to these SpaciMS signals, a rich-phase trigger from the bench reactor was monitored and used in data analysis for temporal alignment of the various species transients.

Analysis of SpaciMS results was based on cycle-averaged data normalized to the calibration location (−2 mm) using the internal Kr standard. Calibration was performed based on standard addition. The elution times for the various species through the SpaciMS sampling capillary can be different, and vary with catalyst temperature and capillary conditioning and geometry. However, elution time was determined to be constant along the catalyst length for a given capillary, species and catalyst temperature. Species-specific elution times were determined for each operating condition using an equivalent blank unwashcoated monolith core. The various species transients were temporally aligned using the bench reactor trigger and measured elution times. The onset time was determined for each temporally aligned species transient as the time where the corresponding signal deviated from the baseline; the onset time is used to temporally sequence the individual transients. The N_2 and NH_3 onset times were determined as the time corresponding to the instantaneous signal being four standard deviations above the baseline. In addition to its unique broadening, greater signal-to-noise ratio (SNR) complicates comparing the H_2 onset time to that of the N species; nevertheless, H_2 onset time was determined as the timing when the instantaneous signal exceeded 650 ppm (i.e., the average N-species concentration at onset scaled by the nominal difference in the SNR values). Lean- and rich-phase NO_x were distinguished, for nitrogen selectivity calculations, based on a model of the measured inlet lean–rich transient scaled to the specific measurement location within the catalyst. Nitrogen selectivity was determined as S/(NO_x + 2*N_2 + NH_3), where S is either NO_x, 2*N_2 or NH_3. Based on effluent measurements, N_2O was negligible at 325 and 400 °C, although 7% N_2O integrated selectivity was indicated at 200 °C. However, the nitrogen balance based on the intra-catalyst measurements excluding N_2O balanced to within ca. 5% over the NSR region. Thus, N_2O is not included in the intra-catalyst nitrogen selectivity calculations presented here.

3. Results and discussion

3.1. Spatial distribution of transient species at 200 °C operation

The distributions of the H_2, N_2 and NH_3 transients through the catalyst for the 200 °C operating condition are shown in Fig. 1a–c; NO_x transients were also acquired but are not shown. The inlet H_2 profile corresponding to the regeneration phase (5 s, 2% H_2) is shown in Fig. 1a. Although the regeneration flow condition is top-hat shaped, the hydrogen profile is bell shaped due to instrument broadening, which is primarily attributable to the capillary sampling used in SpaciMS; the capillary inlet system can be tuned to provide improved temporal resolution. Broadening causes the peak measured H_2 concentration to be below 2%, although the integrated H_2 concentration is equal to the commanded regeneration condition of 10%-s. Another aspect of SpaciMS capillary sampling is the delay of species transients from the regeneration trigger due to elution time of the sample through the capillary. This is apparent for H_2 in Fig. 1a where the species transients appear ca. 35 s after the leading edge of the regeneration trigger due to a constant capillary elution time offset. Although the elution times for NO_x, and N_2 are practically equivalent, the actual H_2 and NH_3 elution times are different and have been calibrated as described in Section 2 above, i.e., in the temporal plots shown in this paper, the species-specific elution times have been calibrated to the N_2 reference timing to allow the various transients to be temporally compared. These characteristics of SpaciMS data (i.e., broadening and elution delay) are applicable to all species.

A portion of the H_2-pulse front is consumed in each differential section of the catalyst as the regeneration pulse travels through the catalyst [10,20,21]. For instance, the amount of H_2 consumed between the 3.2- and 6.4-mm locations is the integral of the difference between the corresponding curves in Fig. 1a. Hydrogen is consumed at the pulse front as apparent in Fig. 1a by the systematic shift in the pulse onset time with increasing distance into the catalyst. In contrast, the H_2-pulse end timing is practically constant, because the tail end of the H_2 regeneration pulse is slipping from location to location within the catalyst. This also causes the timing of the peak H_2 value to be biased to longer cycle times. In general, the H_2-pulse was consumed at early regeneration times and slipped at late regeneration times. This plug-like H_2 consumption trend is indicative of efficient and reductant-supply-limited regeneration as well documented in previous work [6,9,20,23].

The distribution of the N_2 transients through the catalyst is shown in Fig. 1b. In contrast to the H_2-pulse nature, the N_2-pulse onset time is practically constant through the catalyst; this is because N_2 generated at one location slips unreacted to the next location. Locally generated N_2 in each catalyst segment is indicated

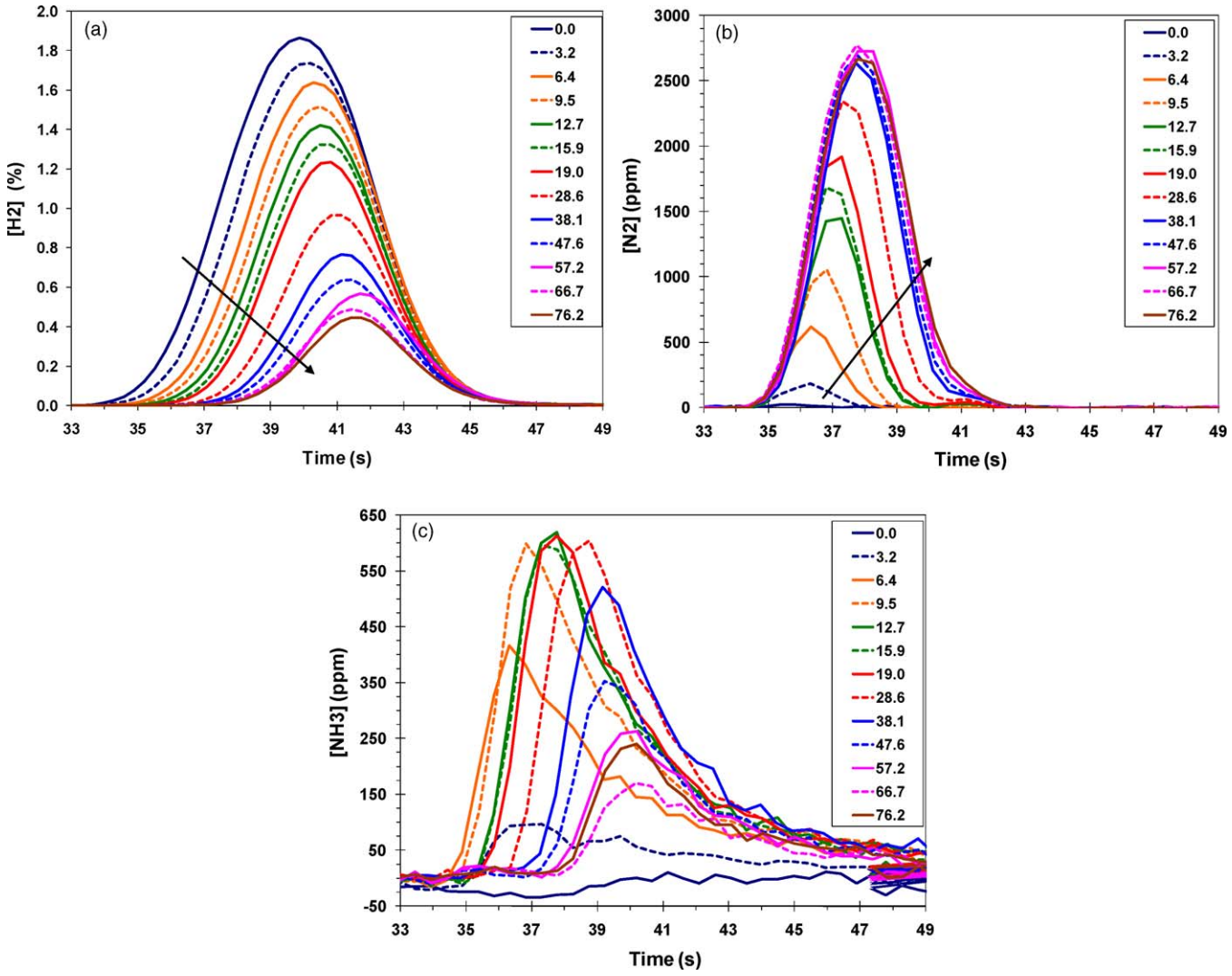

Fig. 1. Species transients at different locations through the catalyst for (a) H_2, (b) N_2 and (c) NH_3 at 200 °C. The legend indicates the specific measurement location in millimeters relative to the catalyst inlet face.

by the difference in the bounding profiles, and is most apparent from the tail end of the corresponding transients. The onset time of the locally generated N_2 is the point where the local transient deviates from that of the previous location; Fig. 1b shows a systematic shift in this time for increasing distance into the catalyst. Nitrogen is generated in each section of the catalyst front half. Less N_2 is generated in the 12.7–15.9-mm section compared to the adjacent sections. The difference observed for hydrogen and nitrogen in terms of temporal profiles demonstrates how the temporal evolution of various species can be substantially different depending on if they are reactants or products; the nature of the H_2 and N_2 transients generally represent the nature of reductants and inert products, respectively. Intermediate species that are both generated and consumed can have further different characteristics as will be apparent from the NH_3 transients. This demonstrates one aspect of how the detailed nature of transient catalysis can be obscured by effluent analysis of integral reactors which does not resolve the detailed timing issues presented here.

The distribution of the NH_3 transients is shown in Fig. 1c. Even though NH_3 is a product like N_2, it shows the nature of a reductant. Specifically, the NH_3 pulse onset time systematically shifts to later regeneration times with increasing distance into the catalyst, and tracks the shift in the H_2 onset time, i.e., the H_2 or regeneration front. In fact, aggressive local NH_3 consumption is apparent from the steep leading edge of the NH_3 transient and the lack of early regeneration time slip, i.e., NH_3 shows the same "plug flow" behavior Mulla et al. [9] observed for H_2, and indicates complete local NH_3 reaction. This suggests that NH_3 is being used for LNT regeneration reactions. Three regions are apparent in Fig. 1c: a "Buildup" region (0–9.5 mm) where local NH_3 generation exceeds consumption, a "Balanced" region (9.5–28.6 mm) where local NH_3 generation and consumption are balanced, and a "Deficit" region (28.6–76.2 mm) where local NH_3 consumption is greater than generation. The leading-edge slope and peak height of the NH_3 transients are approximately constant in the Balanced region.

Less salient aspects of the NH_3 transient are also apparent from Fig. 1c. Little NH_3 is measured in the first 3.2 mm, and the measured transient does not start until after the regeneration front. This could be because either NH_3 generation is delayed, or that intermediate NH_3 is being efficiently consumed. However, the unique SNR disparity at this front location, limits the ability to temporally compare the N_2 and NH_3 transients here. Based on this, it is difficult to detail the role of NH_3 at this very front catalyst location without more measurements throughout this front 3.2-mm section and improved temporal resolution. Another subtle aspect of Fig. 1c is that little difference in the NH_3 transients is observed between the 12.7- and 15.9-mm locations, which is consistent with the N_2 behavior for this same region discussed in

Fig. 1b and the lower NO_x storage in this section (as shown later in Fig. 4). Although the long NH_3 tail observed throughout the catalyst might be interpreted as due to "slow" NO_x sites or competitive H_2O and NH_3 adsorption on Pt [13], it is in fact due to instrument broadening; this is apparent from comparing the normalized transients of Fig. 1c to measured NH_3 pulses using a blank monolith without a catalytic washcoat (not shown). This is not inconsistent with the steep leading edge of the NH_3 transient as it is normal for instruments to have differing pulse-on and pulse-off time constants. These comments on signal tailing and time constant are intended to clarify understanding; specifically, to avoid association of the NH_3 tail with "slow" NO_x sites. However, we do not use these signal characteristics to assess LNT regeneration mechanisms or hypotheses. Finally, the onset time of the NH_3 transient at the catalyst outlet (76.2 mm) is earlier than the previous location and does not follow the established trends of systematically shifting onset time. This is because at the outlet location, effluent from different channels is sampled, and demonstrates that different catalyst channels can have differing performance.

The intra-catalyst transient species distributions described above are generally consistent with those reported by Clayton et al. [13]; they investigated transient species evolution through the catalyst by cutting the catalyst into sections of different lengths. SpaciMS may provide certain benefits such as spatial resolution (particularly very near the catalyst front where regeneration pathway partitioning and changing local NH_3/N_2 ratio may be most evident), and with respect to resolving intra-catalyst transient distributions while maintaining the full monolith section intact.

3.2. Timing of species transients at 200 °C operation

Fig. 2a and b shows the transient species profiles at the 9.5- and 57.2-mm locations, respectively. The H_2, N_2 and NH_3 transients are shown on the same magnitude scale to allow accurate comparison of the different species' relative onset times; however, this causes the H_2 transient to be clipped because of its greater peak magnitude. The distribution at the back end of the catalyst channel (Fig. 2b), as in the effluent, follows the often-reported sequence (N_2, $NH_3 \approx H_2$) which has been the basis for the model of NH_3 being formed at "slow" NO_x storage sites [4,6,7]. However, Fig. 2a shows that NH_3 and N_2 can be generated on similar timescales, and specifically that NH_3 does not always follow N_2. It is clear from Figs. 2a and b and 1c that NH_3 is locally formed and consumed in a plug-like manner along with H_2. Thus, it appears

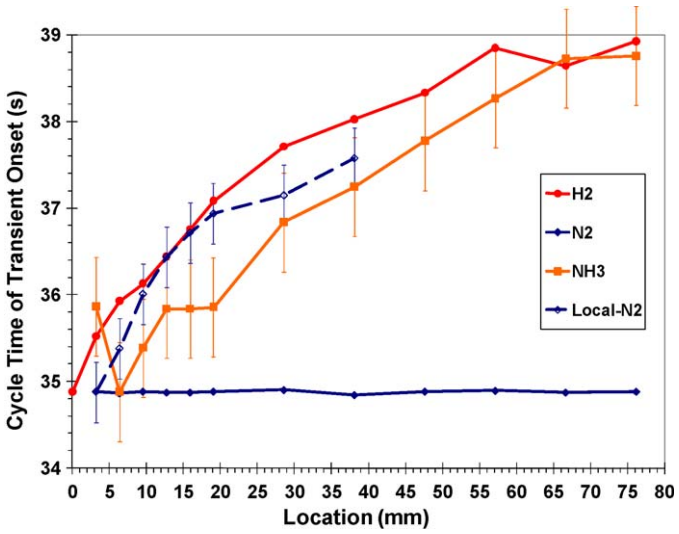

Fig. 3. Distribution of transient onset times for H_2, N_2, local N_2 and NH_3 along the catalyst channel at 200 °C.

that NH_3 is formed and reacts in parallel with H_2 to regenerate LNT NO_x storage sites. This intra-catalyst behavior thus confirms the concept of intermediate NH_3 formation during regeneration of LNT catalysts with H_2 [6,8,9,11–13].

Based on Fig. 2 and the discussions associated with Fig. 1 it is clear that the effluent species sequence is an integral effect. Specifically, the N_2 leading the H_2 and NH_3 in Fig. 2b has slipped from upstream locations where it was generated at early regeneration times. The effectively simultaneous local N_2 and NH_3 generation apparent in Fig. 2a is masked by the integral nature of the catalyst.

The distributions of pulse onset times for H_2, N_2 and NH_3 along the catalyst channel at 200 °C are shown in Fig. 3. The onset time is determined as the time when the signal rises above the baseline as described in Section 2. The intent of Fig. 3 is to quantitatively compare the onset times between the N species, but only the trends in onset times between H_2 and the N species. The onset time for the "local N_2" pulse (i.e., the N_2-pulse without the contribution from slipping N_2) is also shown in Fig. 3, and was determined as the time where the local N_2 transient deviates from that at the previous location as discussed in relation to Fig. 1b. The uncertainty bars (±0.57 s) on the NH_3 profile are the 1-sigma

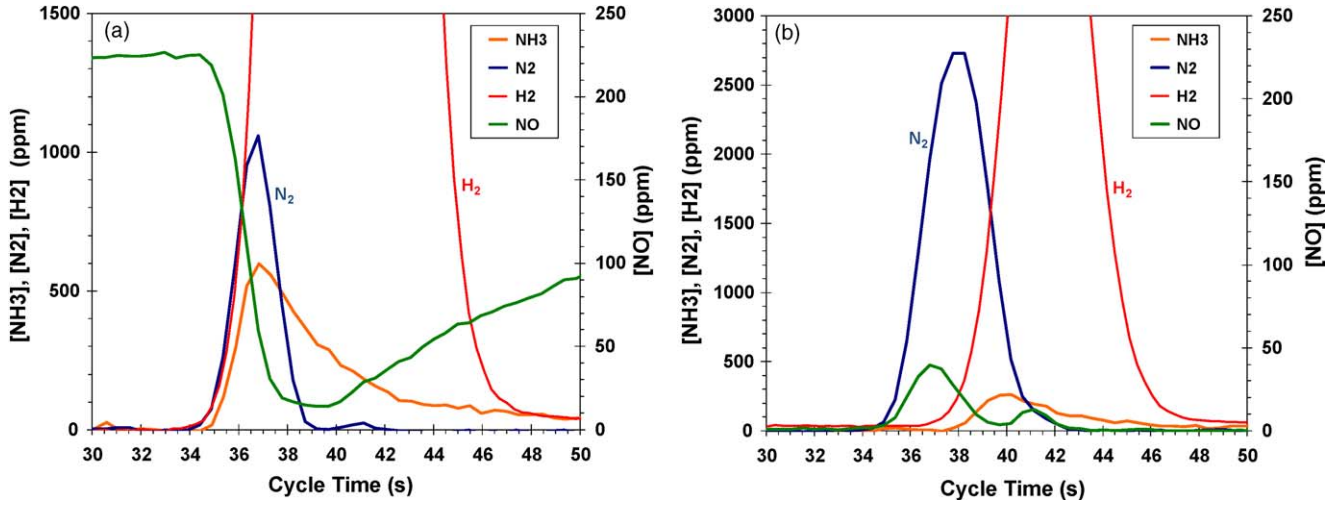

Fig. 2. Transient species profiles at (a) 9.5 mm and (b) 57.2 mm along the catalyst channel at 200 °C.

precision of the NH_3 elution time correction; this is a liberal confidence interval so the NH_3 timing uncertainty is likely somewhat larger. The uncertainty bars (±0.35 s) on the N_2 profile are the nominal precision in the leading edge of the curves in Fig. 1b. Although the NH_3 and N_2 curves generally track and NH_3 onset consistently leads, the base uncertainty of the two profiles practically overlap over the region were N_2 is locally generated. Although no uncertainty bars are shown for the H_2 profile, the corresponding data rate was ca. 0.3 s which is on the same scale as the local-N_2 bars. Accurate measurement of the H_2 onset time and corresponding comparison to that of the N species is complicated by unique broaden and SNR differences discussed earlier. However, the trends (local slope and phase) of the H_2 onset-time profile can be quantitatively compared to that of the N species because the H_2 temporal measurements are precise and a uniform onset-time definition, described in Section 2, is used; changes in H_2 temporal resolution and onset-time definition will only move the H_2 onset-time profile along the temporal axis without changing its local slope or phase. Fortunately, the salient aspect of the H_2 onset-time profile is its local slope or phase and not its accurate value. In general, better temporal resolution is required to accurately sequence the individual species transients. Despite these onset-time uncertainties, the trends of Fig. 3 provide valuable insights to the LNT regeneration chemistry.

The onset-time distributions in Fig. 3 further demonstrate the viability of NH_3-intermediate LNT regeneration pathways via either parallel H_2 and NH_3 regeneration reactions or an exclusively sequential two-step pathway [11–13]. As discussed for Fig. 1, Fig. 3 shows more clearly how the N_2 onset time is constant due to N_2 slip, in contrast to the H_2, NH_3 and local-N_2 onset times, which shift to longer cycle times along the catalyst channel. Moreover, the NH_3-transient onset time generally shifts in parallel with that of the H_2 transient over the region of the catalyst where NO_x is stored (ca. 0–47.6 mm, cf. Fig. 4). This demonstrates that locally generated NH_3 is also locally completely consumed; if this were not the case, then NH_3 would slip from location to location and the phase (w.r.t. timing) shift in the NH_3-pulse onset time would be less than that of the H_2 transient. This tracking of the NH_3 and H_2 onset times indicates that the NH_3 and H_2 are both completely consumed and that both are efficient reductants for NO_x regeneration.

3.3. Cycle-integrated species distribution at 200 °C operation

The cycle-integrated species transients at 200 °C are shown in Fig. 4. For reference, the cycle-integrated inlet catalyst feed is 18,000 ppm-s NO_x and 10%-s H_2. Lean- and rich-phase NO_x are distinguished using the methodology described in Section 2. At 200 °C there is very little rich-phase NO_x, i.e., little NO_x puff or spike. The difference between the inlet (18,000 ppm-s) and local lean-phase NO_x represents the NO_x stored on the catalyst up to that point along the channel. From Fig. 4 it is apparent that ca. half of the NO_x is stored in the first ca. 10 mm of the catalyst, the remaining half is stored in the subsequent ca. 37 mm, and the back ca. 30 mm of the catalyst is not used for NO_x storage. Storage of NO_x is highest in the 2nd and 3rd 3.2-mm sections of the catalyst; 11.3, 18.8, 15 and 11.4% of the inlet NO_x is stored in the front four 3.2-mm sections, respectively, of the catalyst; such a shift in the local NO_x storage peak downstream of the catalyst inlet has been previously demonstrated and attributed to NO oxidation limitations [25,26]. Major growth in the measured net local NH_3 production (cf. Fig. 1c) occurred in the two catalyst regions corresponding to the highest NO_x storage. Furthermore, the lower NO_x storage in the 12.7–15.9-mm section compared to the adjacent sections is consistent with the lower N_2 generation and NH_3 generation/consumption noted in Fig. 1b and c, respectively; this consistently observed axially non-uniform catalyst performance is not uncommon and is likely due to washcoat variations.

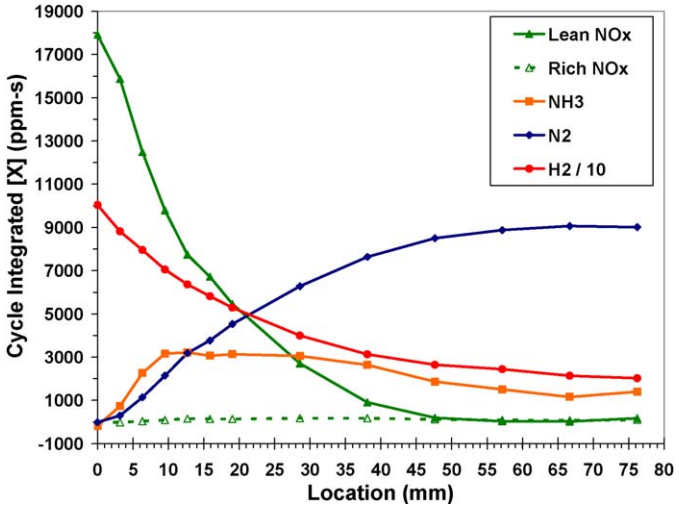

Fig. 4. Cycle-integrated lean-phase NO_x, rich-phase NO_x, H_2, N_2, and NH_3 at 200 °C.

Ammonia increases dramatically in the Buildup region which corresponds to the high-NO_x-density region (0–9.5 mm) of the catalyst. Local NH_3 generation is greater than local consumption in this high-NO_x-density region. Integrated NH_3 is relatively flat in the Balanced region (9.5–28.6 mm), where ca. 45% of the NO_x is stored; this is the same region where in Fig. 1c the NH_3 transients had approximately constant peak height and leading-edge slope. Although integrated NH_3 is relatively constant in this region of more modest stored-NO_x density, it is clear that NH_3 is being consumed from location to location by the varying onset times observed in Figs. 1c and 3; this more clearly demonstrates how local NH_3 generation and consumption are balanced in this catalyst region. Ammonia decreases from 28.6 to 47.6 mm, where the last ca. 14% of the NO_x is stored.

The H_2/NO_x ratio is expected to vary along the catalyst and can affect apparent local NH_3 selectivity. Despite the high NO_x density in the catalyst front, there is also correspondingly high H_2 concentration in this region, and the NH_3 behavior in Fig. 4 suggests a high H_2/NO_x in this region could be responsible for the high NH_3 selectivity [6,8,12,13]. The NH_3 behavior in the 28.6–47.6-mm range suggests either low H_2/NO_x or that a threshold has been reached where NH_3 is consumed to a greater extent than it is locally produced; the distinct leading edges and varying onset times observed for the NH_3 transients of the corresponding curves in Fig. 1c indicate that NH_3 is still being aggressively consumed at the reductant front in this catalyst region. In the back half of the catalyst, NH_3 decreases and approximately follows the H_2 distribution, which is likely due to the reduction of surface oxygen stored on Pt sites.

3.4. Selectivity and temperature effects

In addition to the 200 °C data that has been the basis for the analysis presented thus far, intra-catalyst transient species distributions along the catalyst channel were also measured at 325 and 400 °C. Major features associated with increasing operation temperature were increasing rich-phase NO_x puff and decreasing NH_3 generation. Notably, the 325 °C transient NH_3 profiles were similar to those at 200 °C, but with reduced quantity. Specifically, at 325 °C NH_3 was generated on similar timescales as was N_2 and the temporal phase of the NH_3 front generally shifted in parallel with that of H_2 with increasing distance along the catalyst channel. The nature of the 325 °C NH_3 transient indicated its aggressive utilization for LNT regeneration as detailed with the 200 °C data. As was described for the 200 °C data, the 325 °C

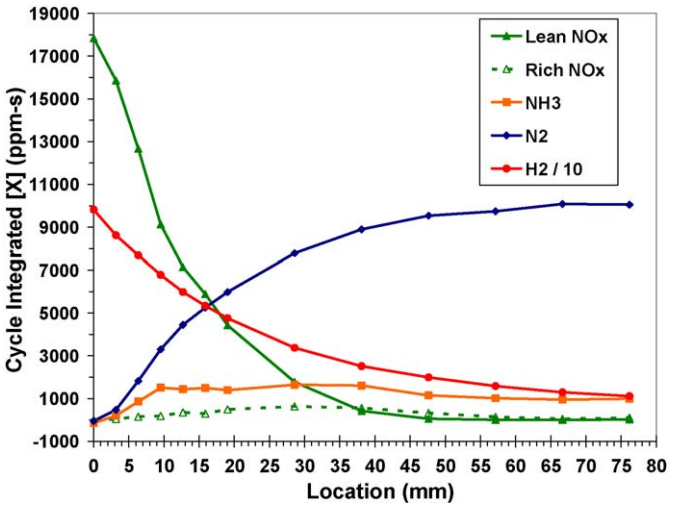

Fig. 5. Cycle-integrated lean-phase NO_x, rich-phase NO_x, H_2, N_2, and NH_3 at 325 °C.

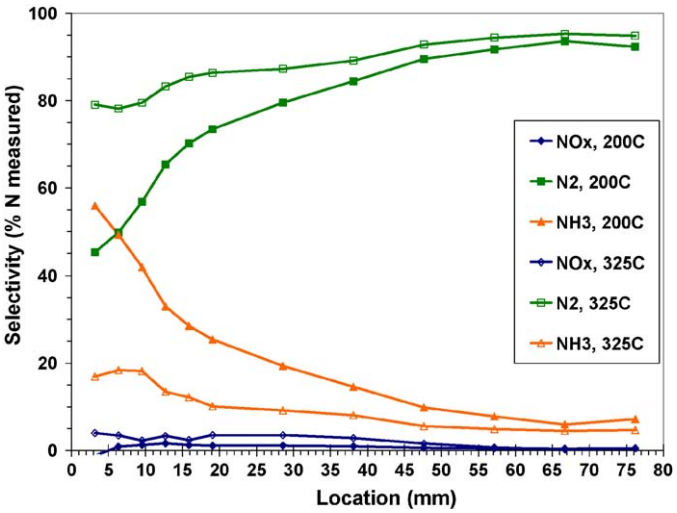

Fig. 6. Nitrogen selectivity distributions along the catalyst channel at 200 °C and 325 °C.

effluent species transients followed the typical (N_2, $NH_3 \approx H_2$) sequence, and were dramatically different from the intra-catalyst and particularly the catalyst-front sequences. Temporal analysis of the 325 °C data follows the 200 °C analysis conclusions, i.e., that LNT regeneration via an Intermediate-NH_3 pathway (either parallel or sequential) is possible and apparent.

The cycle-integrated species transients at 325 °C are shown in Fig. 5. The NO_x storage distribution at 325 °C is practically equivalent to that at 200 °C, which allows relatively clear assessment of temperature effects. The 325 °C NH_3 distributions in Fig. 5 reflects the general features discussed in relation to Fig. 4; an NH_3-Buildup (0–9.5 mm) region at the catalyst front corresponding to a region where ca. 50% of the NO_x is stored, and an NH_3-Balanced (9.5–38.1 mm) region where the remaining NO_x is stored and the integrated NH_3 distribution is flat. In contrast to the 200 °C behavior, at 325 °C the integrated NH_3 is less than N_2 in the NH_3-Buildup region although both species fronts are measured on similar timescales (temporal 325 °C data not shown). Notable increase in the rich-phase NO_x puff at 325 °C is apparent in Fig. 5 compared to Fig. 4.

The equivalent axial distribution of NO_x storage at 200 °C and 325 °C indicates that the regeneration efficiency at these two temperatures is also effectively equivalent. Figs. 4 and 5 also show that the H_2 distribution is effectively equivalent in the NSR region at the two temperatures; this is not inconsistent with varying NH_3 distributions at the two temperatures, as LNT regeneration via Direct-H_2 and Intermediate-NH_3 pathways have the same H_2:N_2 (5:1) and H_2:$Ba(NO_3)_2$ (2.5:1) stoichiometries [11–13]; see Eqs. (1)–(3) in the following section. Temporal analysis has indicated that NH_3 is completely consumed at the transient front in this catalyst region, indicating active and aggressive regeneration via the Intermediate-NH_3 pathway at both 200 and 325 °C. These observations suggest that LNT regeneration may occur through parallel Direct-H_2 and Intermediate-NH_3 pathways, and that the partitioning between the two pathways is different at 200 °C and 325 °C. These results are consistent with previous work showing that NH_3 is equivalently effective to H_2 in regenerating LNT catalyst [8,9,11].

The nitrogen selectivity distributions along the catalyst channel at the various temperatures can be determined using the integrated data, and are shown in Fig. 6. Selectivity to N_2 increases along the catalyst channel at a given operation temperature. Furthermore, N_2 selectivity increases with increasing operation temperature. Selectivity to NH_3 displays the opposite trends to N_2 selectivity. The rich-phase NO_x was significantly greater at 325 °C (more apparent in temporal plots, not shown) which suggests more mobile and/or less stable stored NO_x, and faster NO_x release during regeneration. The selectivity observations are generally in line with previous studies of selectivity dependence on H_2/NO_x ratio [6–8,12,13]. The faster rich-phase NO_x release, and/or more mobile NO_x, with increasing temperature could reduce the H_2/NO_x ratio and be responsible for correspondingly lower NH_3 selectivity.

3.5. Parallel-pathway model of NSR catalyst regeneration

The spatiotemporally resolved species measurements presented here indicate that NSR regeneration via an Intermediate-NH_3 pathway is significant. Moreover, it appears that NSR catalyst regeneration with H_2 proceeds through parallel Dirct-H_2 and Intermediate-NH_3 pathways, following reactions previously proposed [11–13]. The Direct-H_2 pathway proceeds as described in Eq. (1):

$$Ba(NO_3)_2 + 5H_2 \rightarrow N_2 + BaO + 5H_2O, \quad (1)$$

In the Intermediate-NH_3 pathway, NH_3 is produced as described in Eq. (2) and this NH_3 is subsequently used for regeneration reactions as described in Eq. (3):

$$Ba(NO_3)_2 + 8H_2 \rightarrow 2NH_3 + BaO + 5H_2O. \quad (2)$$

$$3Ba(NO_3)_2 + 10NH_3 \rightarrow 8N_2 + 3BaO + 15H_2O, \quad (3)$$

Ammonia decomposition reactions ($2NH_3 \rightarrow N_2 + 3H_2$) can also occur at higher temperatures and influence the selectivity [12,13]; however, this is not expected to occur in the work presented here at 200 and 325 °C. In addition, H_2 and NH_3 can be consumed by oxidation reactions; this was apparent in the data downstream of the NSR region. Notice that the overall stoichiometry is equivalent for the two regeneration pathways, and thus pathway partitioning cannot be assessed by local stoichiometry distributions; particularly for the complex transient experiments presented here. The partitioning between the parallel regeneration pathways appears to be controlled by the local H_2/NO_x ratio, in a manner consistent with that reported in the literature for NH_3 selectivity, and may vary along the catalyst. Specifically, the equivalent stored-NO_x and H_2 distributions at 200 and 325 °C combined with the greater rich-phase NO_x puff at 325 °C is expected to lower the local H_2/NO_x ratio at 325 °C; this is consistent with the observed lower NH_3 at 325 °C in light of the dependence of NH_3 selectivity on H_2/NO_x ratio

reported in the literature [6,8,9]. The overall regeneration effectiveness does not vary with partitioning between the parallel pathways for the conditions reported here. It may be possible to more clearly understand the significance of the two regeneration pathways via higher temporal and spatial resolution measurements just inside the catalyst inlet face with minimal interference from integral-reactor effects.

4. Conclusions

We have characterized the transient species distributions along a catalyst channel under realistic LNT cycling conditions at different temperatures. This work has demonstrated the ability to make intra-catalyst measurements of transient NH_3 distributions, and expands the broad SpaciMS species applicability previously demonstrated for other major LNT species. With these unique measurements, we have assessed the NH_3 formation and utilization along the catalyst in light of existing theories.

The timing of transient NH_3 emissions at 200 °C is very different at the catalyst exit compared to that inside the catalyst. In the catalyst effluent we observe the typical species sequence (N_2, $NH_3 \approx H_2$). However, we have shown that NH_3 is generated on similar timescales as N_2 in the catalyst front, where ca. 70% of the NO_x is stored. This demonstrates that NH_3 can be generated on fast timescales, and that indirect H_2 regeneration via Intermediate-NH_3 pathway is possible.

The nature of the NH_3 transients at 200 °C varies along the catalyst and can be used to assess NH_3 utilization. The systematic shift in the transient onset time with increasing distance into the catalyst and the steep leading-edge slope indicate that NH_3 is being locally generated and consumed, and that NH_3 is not slipping from location to location at the reductant front in the NSR region. Combined with the temperature-dependant behavior, the tracking of the NH_3 and H_2 onset times indicates that both NH_3 and H_2 are aggressively consumed at the reductant front for LNT regeneration. This indicates that LNT regeneration via an Interfediate-NH_3 pathway occurs.

Three distinct NH_3 zones are apparent through the catalyst. In a Build-up zone, in the catalyst front were ca. 50% of the NO_x is stored, the cycle-integrated NH_3 increases from location to location. More NH_3 is generated than consumed in this front catalyst zone. In a Balanced zone, downstream of the Build-up zone and where most of the remaining NO_x is stored, the cycle-integrated NH_3 is flat. There is a balance between local NH_3 generation and utilization from location to location in this zone. In the back end of the catalyst not used for NO_x storage, a Depletion zone exists where the cycle-integrated NH_3 is consumed apparently by surface oxygen.

Increasing the operation temperature from 200 to 325 °C decreases NH_3 selectivity. A corresponding increase in the rich-phase NO_x slip, i.e., NO_x puff, is also observed with this temperature increase. This suggests more mobile NO_x at higher temperatures and corresponding lower H_2/NO_x ratios. This further suggests that the conventional trend of lower NH_3 selectivity with lower H_2/NO_x is followed.

Although the NO_x storage and H_2 utilization distributions are practically equivalent at 200 and 325 °C, the corresponding NH_3 distributions are markedly different. However, NH_3 is aggressively consumed at the reductant front in the NSR zone at both temperatures. This behavior suggests that LNT regeneration occurs through parallel Direct-H_2 and Intermediate-NH_3 pathways, and that the apparent partitioning between the two paths varies with temperature. Furthermore, regeneration is equivalently efficient at the two temperatures regardless of the partitioning between the two pathways. This is consistent with previous studies that have shown equivalent reductive efficiency of H_2 and NH_3.

This work clarifies the complex chemistry occurring within the NSR zone of an LNT catalyst and how it can be markedly different from that observed in the catalyst effluent. A complex reaction network exists in the high-NO_x-storage-density catalyst front including NH_3 generation, H_2 and NH_3 oxidation, and parallel Direct-H_2 and Intermediate-NH_3 regeneration pathways, with pathway partitioning varying with temperature. Without intra-catalyst measurements, these rich details are obscured, and so is corresponding detailed catalyst reaction understanding. We have used these intra-catalyst measurements to better understand NH_3 formation and utilization. We believe that by implementing models of the complex reaction network along with intra-catalyst measurements, the reaction details such as partitioning of the regeneration pathways can be further clarified.

Acknowledgments

This research was performed in a Cummins-ORNL CRADA sponsored by the U.S. Department of Energy, Vehicle Technologies Program, with Ken Howden and Gurpreet Singh as the Program Managers. We thank Mr. Neal Currier and Dr. Aleksey Yezerets of Cummins, Inc., Dr. John Breen (formerly) of Queen's University Belfast, Mr. Josh Pihl, Dr. Jim Parks, Dr. John Storey and Dr. Stuart Daw at ORNL for useful discussions and Dr. Todd Toops of ORNL for H_2 chemisorption and BET measurements and discussion.

References

[1] W.S. Epling, L.E. Campbell, A. Yezerets, N.W. Currier, J.E. Parks II., Catal. Rev. -Sci. Eng. 46 (2004) 163–245.
[2] T. Lesage, C. Verrier, P. Bazin, J. Saussey, M. Daturi, Phys. Chem. Chem. Phys. 5 (2003) 4435–4440.
[3] T. Lesage, C. Verrier, P. Bazin, J. Saussey, S. Malo, C. Hedouin, G. Blanchard, M. Daturi, Top. Catal. 30/31 (2004) 31–36.
[4] L. Castoldi, I. Nova, L. Lietti, P. Forzatti, Catal. Today 96 (2004) 43–52.
[5] J. Parks, S. Huff, J. Pihl, J.-S. Choi, B. West, SAE Technical Paper 2005-01-3876, 2005.
[6] J.A. Pihl, J.E. Parks II, C.S. Daw, T.W. Root, SAE Technical Paper 2006-01-3441, 2006.
[7] I. Nova, L. Castoldi, L. Lietti, E. Tronconi, P. Forzatti, Top. Catal. 42–43 (2007) 21–25.
[8] L. Cumaranatunge, S.S. Mulla, A. Yezerets, N.W. Currier, W.N. Delgass, F.H. Ribeiro, J. Catal. 246 (2007) 29–34.
[9] S.S. Mulla, S.S. Chaugule, A. Yezerets, N.W. Currier, W.N. Delgass, F.H. Ribeiro, Catal. Today 136 (2008) 136–145.
[10] J.-S. Choi, W.P. Partridge, J.A. Pihl, C.S. Daw, Catal. Today 136 (2008) 173–182.
[11] I. Nova, L. Lietti, P. Forzatti, Catal. Today 136 (2008) 128–135.
[12] L. Lietti, I. Nova, P. Forzatti, J. Catal. 257 (2008) 270–282.
[13] R.D. Clayton, M.P. Harold, V. Balakotaiah, Appl. Catal. B 84 (2008) 616–630.
[14] Material Safety Data Sheet information, e.g., www.mathesontrigas.com/MSDS/index.aspx.
[15] M.M. Baum, E.S. Kiyomiya, S. Kumar, A.M. Lappas, V.A. Kapinus, H.C. Lord, Environ. Sci. Technol. 35 (2001) 3735–3741.
[16] J.H. Seinfeld, S.N. Pandis, Atmospheric Chemistry and Physics, Wiley and Sons, NY, 1998, p. 433.
[17] W.P. Partridge, J.M.E. Storey, S.A. Lewis, R.W. Smithwick, G.L. DeVault, M.J. Cunningham, N.W. Currier, T.M. Yonushonis, SAE Technical Paper 2000-01-2952, 2000.
[18] H. Hu, J. Reuter, J. Yan, J. McCarthy, Jr., SAE Technical Paper 2006-01-3552, 2006.
[19] N. Satoh, H. Ohno, T. Nakatsuji, in: Proceedings of 15th Aachen Colloquium Automobile and Engine Technology, October, 2006, pp. 259–270.
[20] J.-S. Choi, W.P. Partridge, C.S. Daw, Appl. Catal. B 77 (2007) 145–156.
[21] J.-S. Choi, W.P. Partridge, C.S. Daw, Appl. Catal. A 293 (2005) 24–40.
[22] W.P. Partridge, T.J. Toops, J.B. Green, T.R. Armstrong, J. Power Sources 160 (2006) 454–461.
[23] J.-S. Choi, W.P. Partridge, W.S. Epling, N.W. Currier, T.M. Yonushonis, Catal. Today 114 (2006) 102–111.
[24] J.P. Breen, R. Burch, C. Hardacre, C.J. Hill, C. Rioche, J. Catal. 246 (2007) 1–9.
[25] K. Aftab, J. Mandur, H. Budman, N.W. Currier, A. Yezerets, W.S. Epling, Catal. Lett. 125 (2008) 229–235.
[26] W.S. Epling, A. Yezerets, N.W. Currier, Catal. Lett. 110 (2006) 143–148.